sustainability

MDPI

Article

Strengthening of Masonry Structures by Sisal-Reinforced Geopolymers

Luigi Palizzolo *, Carmelo Sanfilippo, Sana Ullah and Salvatore Benfratello

Department of Engineering, University of Palermo, Viale delle Scienze, Bd 8, 90128 Palermo, Italy; carmelo.sanfilippo01@unipa.it (C.S.); sana.ullah01@unipa.it (S.U.); salvatore.benfratello@unipa.it (S.B.)
* Correspondence: luigi.palizzolo@unipa.it

Abstract: The development of alternative environmentally friendly and sustainable materials in the construction industry has become a fundamental area of research. The current cementitious materials used in existing retrofitting techniques for masonry structures are unsustainable from an environmental point of view. The geopolymer, as a suitable alternative to ordinary Portland cement (OPC), has attracted interest in the last 20 years due to its environmental sustainability and improved properties compared to conventional concrete. To improve the ductile behavior of geopolymers, the adoption of fibers has been widely proposed in the scientific literature for a broad range of applications. The adoption of natural fibers can make geopolymers more advantageous based on their intrinsic environmental sustainability. The aim of this paper is to validate the performance of sisal fiber-reinforced geopolymer plaster as a strengthening material for masonry structures, which will be achieved by modeling the mechanical behavior of geopolymer samples in two different phases. The first phase accounts for the experimental results suitably obtained in the laboratory, while the second phase models the behavior of a masonry panel reinforced with geopolymer plaster using a suitable FEM model in Abaqus.

Keywords: ordinary Portland cement; geopolymer; sisal fiber; strengthening; masonry structures; FEM modeling; sustainability

Citation: Palizzolo, L.; Sanfilippo, C.; Ullah, S.; Benfratello, S. Strengthening of Masonry Structures by Sisal-Reinforced Geopolymers. *Sustainability* **2024**, *16*, 9181. https://doi.org/10.3390/su16219181

Academic Editor: Dušan Katunský

Received: 10 September 2024
Revised: 15 October 2024
Accepted: 21 October 2024
Published: 23 October 2024

1. Introduction

Historic masonry heritage constitutes a fundamental part of the global and Italian heritage, which must be adequately preserved from structural, restoration and sustainability points of view. In this framework, a fundamental role is played by suitable innovative materials that can be adopted both in the restoration and structural retrofitting phases (see, e.g., [1–4]). Masonry building heritage is constituted by different typologies of masonry (e.g., tuff ashlar masonry, rubble masonry, stone masonry). Masonry reuse can play a key role in sustainability, especially in terms of environmental characteristics, since it reduces the need for new construction projects, and the consequent energy and water consumption and waste production. However, masonry structures are vulnerable to natural hazards such earthquakes due to their intrinsic weakness in resisting lateral loads which generate tensile stresses in the material. Therefore, continuous maintenance/repair is required to maintain their structural properties. The vulnerability of existing historical masonry structures was recurrently observed under both static and dynamic loads, specifically in the aftereffects of recent Italian seismic events (see, e.g., [5,6]).

Actually, the evolution of the structural standard codes in the topic of dynamic structural analysis (see, e.g., [7–10]) and design (see, e.g., [11–14]) requires more and more in-depth study on the performance of both new and existing structures.

Traditional existing buildings stocks are made of stone and brickwork masonry and do not comply with the actual design codes and standards. Due to the poor performance under lateral loads during earthquakes, the structural safety of masonry buildings is a challenging

task for engineers, architects and restorers. Indeed, many studies have been devoted to enhancing the structural capacity of masonry buildings to enable them to withstand seismic actions according to the more recent international standards.

The most utilized interventions are (1) the reinforcement of the masonry panel with appropriately designed layers of plaster (see, e.g., [15–17]); (2) the insertion of steel frames in the existing opening of the panel, often equipped with special devices to optimize the global behavior of the involved masonry panel (see, e.g., [18–25]). Masonry structures are intrinsically able to mainly absorb compression loadings, showing only [26] a very limited resistance capacity under tension loadings.

The load-bearing walls of masonry structures are subjected to in-plane shear forces and out-of-plane bending during earthquakes; the out-of-plane capacity can be enhanced by improving wall-to-floor and wall-to-wall connections, as seismic forces will possibly be transferred from face-loaded walls to return walls. However, in-plane failure causes sliding, shear, rocking or toe failure, and therefore, techniques and materials for restoration and strengthening need to be developed [27–29]. Several retrofitting methodologies for masonry structures are available, among which the most adopted are (1) repointing (see, e.g., [30–33]); (2) grout/epoxy injection (see, e.g., [34]); (3) shotcrete (see, e.g., [35,36]); (4) FRPs (see, e.g., [37]); (5) mesh reinforcement and junction strengthening (see, e.g., [38]). However, the material used in these methodologies and the related production of waste [39] make these methodologies unsustainable from an environmental point of view.

Structural plaster on the walls of existing masonry structures can be adopted to improve the load-bearing ability in both horizontal and vertical actions and for thermal insulation [39,40]. Due to many environmental aspects, cement plaster is unsustainable, and therefore, alternative binders (i.e., binders more sustainable from an environmental point of view) need to be developed. Clearly, a specific focus on the compatibility with existing materials and the improvement in the load-bearing capacity [40,41] has to be considered. The development of advanced materials in recent years and the related numerical and theoretical modeling of their mechanical behavior provide alternative solutions such as, for example, bio-composites [42] and natural or artificial fiber-based geopolymer plaster/mortar.

The development of alkali-activated mortars without cement (geopolymer mortar) utilizes waste materials and shows exceptional properties for the conservation and restoration of existing masonry structures [43] in terms of fresh and hardened stages [44], durability in aggressive environments [45] and a low environmental impact [46].

Geopolymers can be developed from alumino silicate source materials (fly ash or slag) with alkaline activators and natural materials such as kaolinite clay, rice husk ash, quarry dust, etc. [47]. The chemical reaction is geopolymerization [48] and the most common used alkaline activators are sodium hydroxide (NaOH), sodium silicate (Na_2SiO_3), potassium hydroxide (KOH) and potassium silicate (K_2SiO_3) [49]. From the above remarks, it follows that geopolymers are environmentally friendly [50].

Despite all of the advantages reported above, geopolymers show brittle behavior, like ordinary Portland cement. To tackle this drawback and to enhance the ductile behavior of geopolymers, many studies have focused on the development, characterization and implementation of fiber-reinforced geopolymers. Fiber-reinforced geopolymers can be used as an effective retrofit material for the strengthening of masonry structurers with higher durability, better mechanical and structural properties, and an adequate insulating and thermal capacity as well [51–54]. However, the selection of fibers for reinforcement is a demanding task since it must consider the compatibility between the fibers and material properties; from a structural point of view, proper fiber–matrix interactions for stress transmission and an optimum aspect ratio to resist post-cracking behavior are two fundamental features to be considered. To improve mechanical performance, pre-treatment by water run-off and alkali treatment in NaOH solution can be adopted to induce a rough surface for better binding and adhesion between the matrix and fibers [55–59]. As reported in [60,61], the performances of fiber-reinforced geopolymers are more dependent on the material

properties of fibers rather than the binders, emphasizing the crucial role of fiber selection. The mixing process between fibers and the matrix is another crucial task requiring suitably defined procedures to achieve uniform fiber addition, and it depends on the geometry, content and fiber type [60,62]. Increasing the fiber content reduces the workability of the composite due to the increase in viscosity and yield stress [63], and it also has important effects on the mechanical behavior.

In terms of mechanical characteristics, the geopolymer's compressive strength is a major parameter and its value depends on brittleness, micro-crack distribution, pore structure and boundary conditions. In the literature, a standard code of practice to be adopted for the design of the geopolymer matrix is available [64]. In general, the better mechanical properties of geopolymers are observed for a fiber content of less 2% due to the increase in porosity above the critical fiber content (usually between 0.2 and2%) [65,66], but this critical value strongly depends on the fiber type and on the selected precursor. The increment in mechanical characteristics (toughening mechanism, ductility and energy absorption) depends on the fiber–matrix interaction, on the fiber nature and on the fiber-to-binder interaction [67–70].

Each type of fiber in the geopolymer has certain limitations and specific advantages. For environmental issues and the development of sustainable materials, many researchers have recently put their efforts toward the utilization of natural fibers for the reinforcement of geopolymer-based materials. Natural mono-filament cellulosic fibers like hemp, kenaf, bagasse, sisal and jute are considered alternatives to synthetic fibers in the matrix due to their low density, cost, acceptable properties and reduced thermal conductivity [71–74]. The improvement in the mechanical characteristics of fiber-reinforced geopolymers due to the adoption of natural fibers is reported in many papers (see e.g., [75–77]). Recently, the numerical modeling of the mechanical behavior of sisal-reinforced geopolymer mortar has been investigated to define the suitable material model to be adopted in subsequent structural FEM analyses [78].

The initial aim of this paper is to assess the opportunity of using natural fiber-reinforced geopolymer plaster to improve the structural response of masonry structures. This goal is achieved by focusing the attention specifically on sisal fibers for reinforcement by performing appropriate experimental trials to depict the mechanical response of the reinforced geopolymer, by obtaining a numerical model of this material and by performing a structural analysis of a masonry panel with and without the use of sisal fiber-reinforced geopolymer plaster. The results of the masonry panel are compared with those developed using a standard approach to obtaining reinforced plaster to confirm the effectiveness of the sisal-reinforced plaster in increasing the structural response of masonry.

2. Materials and Methods

2.1. Specimen Preparation, Mechanical Tests and Material Numerical Modeling

The geopolymer matrix was developed by adopting metakaolin as the precursor with a silicon-to-aluminum (Si/Al) ratio of 1.3:1 and a particle size distribution ranging between 1 and 100 μm. The alkaline activator used was 7M potassium hydroxide (KOH), prepared by mixing potassium silicate (K_2SiO_3) powder and KOH pellets with 99% purity with deionized water. The maximum diameter of the fine aggregate particles used was 2 mm, and the commercial reagents were supplied by Carlo Erba Reagents (Italy). The source of the sisal plants was a plantation in northern Sicily, where the extracted fibers were collected, washed and dried for 48 h at 25 °C. From a literature review, it is observed that the mechanical properties of a composite are highly dependent on the replacement percentage of natural fibers. In this paper, we adopted a replacement of 2% weight content of the aggregate with short sisal fibers 25 mm in length. The geopolymer samples were prepared by initially mixing the powders, followed by the addition of the alkaline activator. Subsequently, sisal fibers were incorporated into the mortar using a mechanical mixer for ten minutes. The chemical composition of metakaolin is reported in Table 1; the mixture ratio is 1 (precursor):2 (river sand).

Table 1. Chemical composition of metakaolin.

Element	Wt %
C K	2.20
O K	39.53
AlK	27.22
SiK	29.71
TiK	1.34

The selected value of replacement agrees with the results reported in [79]. The mechanical behavior of the sisal fiber-reinforced geopolymer matrix was analyzed by conducting compression, three-point bending and splitting (Brazilian indirect tensile) tests. The EN 1015-11 [80] standard was followed for the compression and bending tests, while the ASTM D3967 standard [81] was adopted for the splitting test. The specimens' dimensions were 160 mm × 40 mm × 40 mm for the bending test (Figure 1a), while cylindrical samples with a nominal diameter and thickness of 50 mm were adopted for the splitting test (Figure 1b). The compression tests were performed on cube specimens with each side equal to 40 mm obtained by cutting the wrecked half parts at the end of the bending test (Figure 1c). All of the samples were cured at room temperature for the duration of 28 days. In the three-point bending test, the length of span was fixed equal to 100 mm. The Universal testing machine (UTM) model ETM-C (WANCE, Shenzhen, China), equipped with a 50 kN load cell, was used for performing the mechanical tests, and a pre-load of 10 N was applied before the recording of data. The tests were performed under displacement control, at a rate of 1 mm/min for bending and 0.5 mm/min for compression, while stress control was adopted for the splitting test with a rate equal to 0.05 MPa/sec. For each batch, three specimens were casted and tested for each mechanical test. To collect the strain data during testing, samples were equipped with a HBK strain gauge (K-CLY4, 120 Ohm, 6 mm measurement grid). The HBK MGC Plus data acquisition system driven by MGC Plus assistant was adopted for the recording of strain and acting load.

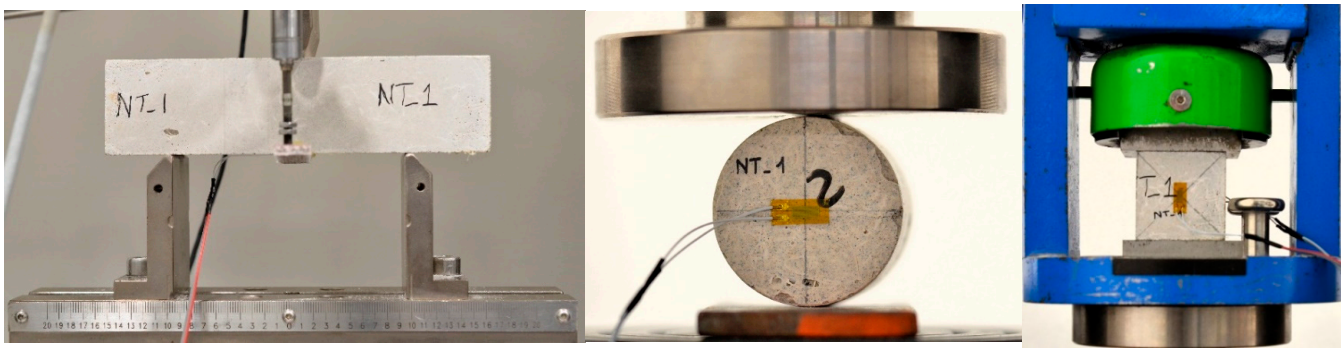

(**a**) (**b**) (**c**)

Figure 1. Experimental setup: (**a**) three-point bending test; (**b**) splitting test; (**c**) compression test.

The experimental results in terms of compression of the stress—train curve behavior and ultimate tensile strength were adopted as the input information for developing the ABAQUS 2017 input data. The concrete damaged plasticity (CDP) material model available in the ABAQUS 2017 library was selected and the CDP Generator tool [82] was used to gather the information required by the ABAQUS 2017 material model. The input data for this tool were obtained from the experimental data. Subsequently, the above-mentioned experimental tests were modeled in ABAQUS 2017 [83] (C3D8R 3D element, mesh size equal to 1 mm, contact between steel and samples with 0.15 friction coefficient, and penalty friction formulation), adopting the same sample dimensions as in the experimental tests and performing the test control equal to that adopted in the corresponding experimental one.

2.2. Numerical Analysis of Masonry Panel

The structural application of sisal fiber-reinforced geopolymers was investigated by adopting a masonry panel scheme, as shown in Figure 2. The geometry details of the two examined panels are presented in Table 2, together with the mechanical ones corresponding to the available mean values available in Table C8.5.I of [84]. The two different masonry panels studied are characterized by masonry with split stone (Masonry 1) and ashlar masonry with regular squared blocks (Masonry 2). The aim of these analyses is to validate the beneficial effects of plaster realized by the sisal fiber-reinforced geopolymers (in the following, referred to as the proposed plaster) on the overall mechanical behavior of the panel. To this end, the typical panel was subjected to a uniformly distributed vertical load q, as shown in Table 2, and to a horizontal load F, whose value ranges from 0 to the collapsed one. The load F was applied as the resultant of pressure of an appropriate value applied on the steel plate. The panel was analyzed by using the ABAQUS FEM environment, assuming a CDP material model and C3D8R 3D elements. The required CDP parameters in ABAQUS were derived from the mechanical ones reported in Table 2, always adopting the CDP Generator tool, assuming a tensile strength equal to 0.1 the compressive one and a linear behaviour, as it is usual in the modelling of the mechanical behaviour of cementitious materials, for the fracture energy obtained by the experimental splitting test.

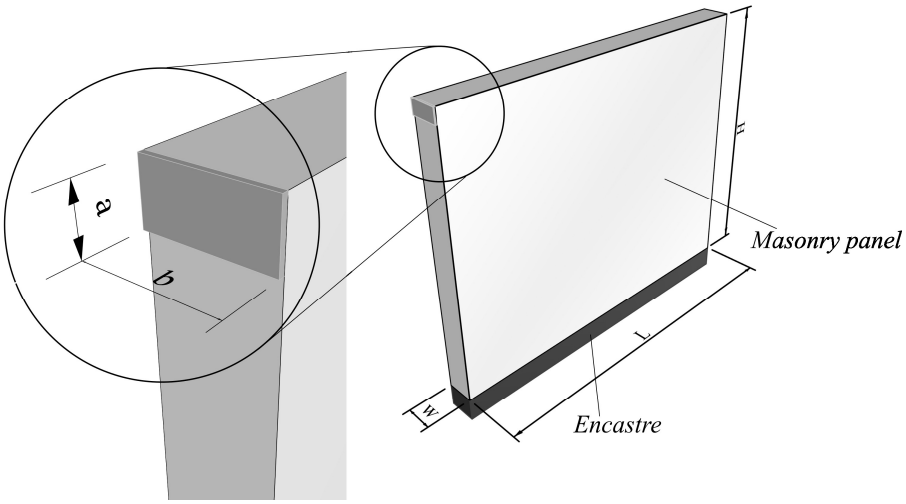

Figure 2. Masonry panel under examination: (**a**) plate height; (**b**) plate base.

Table 2. Adopted geometrical and mechanical parameters.

Parameter	Masonry 1	Masonry 2
Length L [m]	5.0	5.0
Height H [m]	4.0	4.0
Thickness w [m]	0.4	0.4
Plate height [m]	0.2	0.2
Plate base [m]	0.4	0.4
Distributed load q [kN/m]	90	130
E [MPa]	1250	2400
G [MPa]	410	800
w [kN/m^3]	20	22
f_c [MPa]	2.0	6.0
τ_0 [MPa]	0.05	0.09

The boundary conditions were assumed as fully restrained at the panel bottom, while at the top of the panel, only the displacement along the length of the panel was allowed. Three different conditions were analyzed for each masonry: a simple masonry panel, a masonry panel with standard reinforced plaster (obtained by correcting the mechanical

parameters of the masonry as in Table C8.5.II of [84]) and a masonry panel with the proposed plaster with 0.03 m thickness (usual value of plaster thickness adopted in practical application). The masonry panel with the proposed plaster was analyzed by assuming perfect kinematical compatibility between the plaster and masonry. The mesh size for the FE analysis of the panels is equal to 0.1 m and it was selected after a sensitivity analysis to obtain the optimal value in terms of numerical effort and the accuracy of the results. Specifically, the adopted mesh size leads to a computational time equal to about 7 min with an HP i7 32GB RAM workstation, while a halved mesh leads to about 35 min of computational time with a difference equal to 2% in terms of top displacement.

3. Results and Discussion

The first step is to check the feasibility of the CDP material model and that of the FEM model to reproduce the experimental results. It is important to note that the CDP material model is usually adopted for modeling the behavior of homogeneous concrete-like materials. On the other hand, the material studied in the experimental tests is a concrete-like material reinforced with sisal fibers (i.e., not homogeneous in a narrow sense) and, as is well known, the presence of the fibers strongly affects the mechanical behavior, especially when tensile stresses arise due to their stitching effect. Therefore, the novelty of this paper is to evaluate the adoption of the CDP model in the case of fiber-reinforced concrete-like materials. Beside the mechanical characteristics (stiffness and strength both in compression and in tension), a further critical parameter to obtain accurate results is the adhesion between the fibers and matrix which strongly influences the post-elastic behavior. This topic is outside the aim of this paper, and it will be studied in a future experimental and numerical campaign. It is important to note that in the proposed reinforced plaster, the fibers are randomly distributed inside the matrix. The design of a suitable numerical model able to consider the real distribution and the adhesion between the fibers and matrix is a very complex task and is outside the aim of this paper. Further, the possible advantages of the results obtained by such a numerical model should be compared with the unavoidable hugely increased computational effort. In Figure 3a, the compression stress f_c obtained from the experimental test and that obtained from the numerical model is sketched and compared, showing very good agreement both in the elastic range and in the plastic one. In this test, the influence of the fibers is not evident since the overall mechanical behavior is governed by the mechanical characteristics of the matrix. In a similar way, in Figure 3b, the stress calculated from the experimental splitting test f_{st} is sketched and compared with that arising from the numerical model. In this case, the numerical results are satisfactory in the elastic range and less satisfactory in the plastic range. This can be ascribed to the role of the fiber in the specific (splitting) test which is very difficult to be described by a numerical model for homogeneous materials. In this case, the stitching effect of the fibers is limited since the tensile stresses are concentrated in a limited zone of the specimen. Finally, as for the compression and splitting tests, in Figure 3c, the bending stress f_b derived from the experimental test is reported together with that arising from the numerical model. Also, in this case, the numerical model gives satisfactory results, especially in the elastic range, while those in the plastic range are effected by an error; the latter is reduced with respect to the case of the splitting test and it can be ascribed again to the fibers and, in particular, to their stitching role during the bending test, which is more evident since the part of the specimen where tensile stresses arise is wider than in the case of the splitting test. The above remarks allow us to state that the CDP material models in a satisfactory way the experimental behavior of sisal-reinforced geopolymers, and consequently, it can be adopted for the subsequent numerical analyses of the masonry panels.

As described above, the subsequent step is to perform the analysis of the mechanical behavior of the masonry panels. As is usual in structural engineering, the overall performance of a masonry panel is evaluated in terms of the pushover $F-\Delta$ curve, with F being the applied load and Δ being the corresponding displacement of the reference point that, in the case under examination, is the middle one of the upper right edge of the investigated

panel. The obtained results are presented in Figure 4. The analysis of these figures shows the crucial role of the studied interventions in the increment in the mechanical behavior of the masonry panel, especially in terms of ultimate load. However, it must be noted that the proposed plaster leads to an increment in the overall response greater than the corresponding one arising from the adoption of the standard reinforced plaster as in [81]. This increment, however, is not equal for the two masonries under investigation, as that for Masonry 1 (about 1.5 times) is greater than that for Masonry 2 (about 1.3 times). This remark, together with the fact that the modulus of elasticity of Masonry 2 is 2.07 times that of Masonry 1, leads to the further observation that the overall structural efficacy of the proposed plaster increases with the increment in the ratio of E_p/E_m, with E_p being the modulus of elasticity of the proposed plaster and E_m that of the masonry. Another important remark is that the proposed plaster is sustainable from an environmental point of view, while the materials usually adopted in reinforced plaster as in [80] are not sustainable.

Among the available output parameters of the ABAQUS FE model, two of them give a measure of the damage suffered by the material. These parameters, referred to as d_c and d_t for compression and tension, respectively, range from 0 (no damage) to 1 (fully damaged), and their meaning is related to the deterioration of the material stiffness in the softening phase as it can be easily derived from the examination of Figure 5 [83].

To perform a further check on the effectiveness of the proposed plaster for the strengthening of masonry structures, the above-described parameters d_c and d_t are sketched in the following figures for the studied masonry panels. These maps are related to the damage of the material constituting the core of the analyzed masonries, i.e., the panel itself in the case of the original panel and in that of the standard reinforced one or the panel without the plaster in the case of the panel reinforced by the proposed plaster.

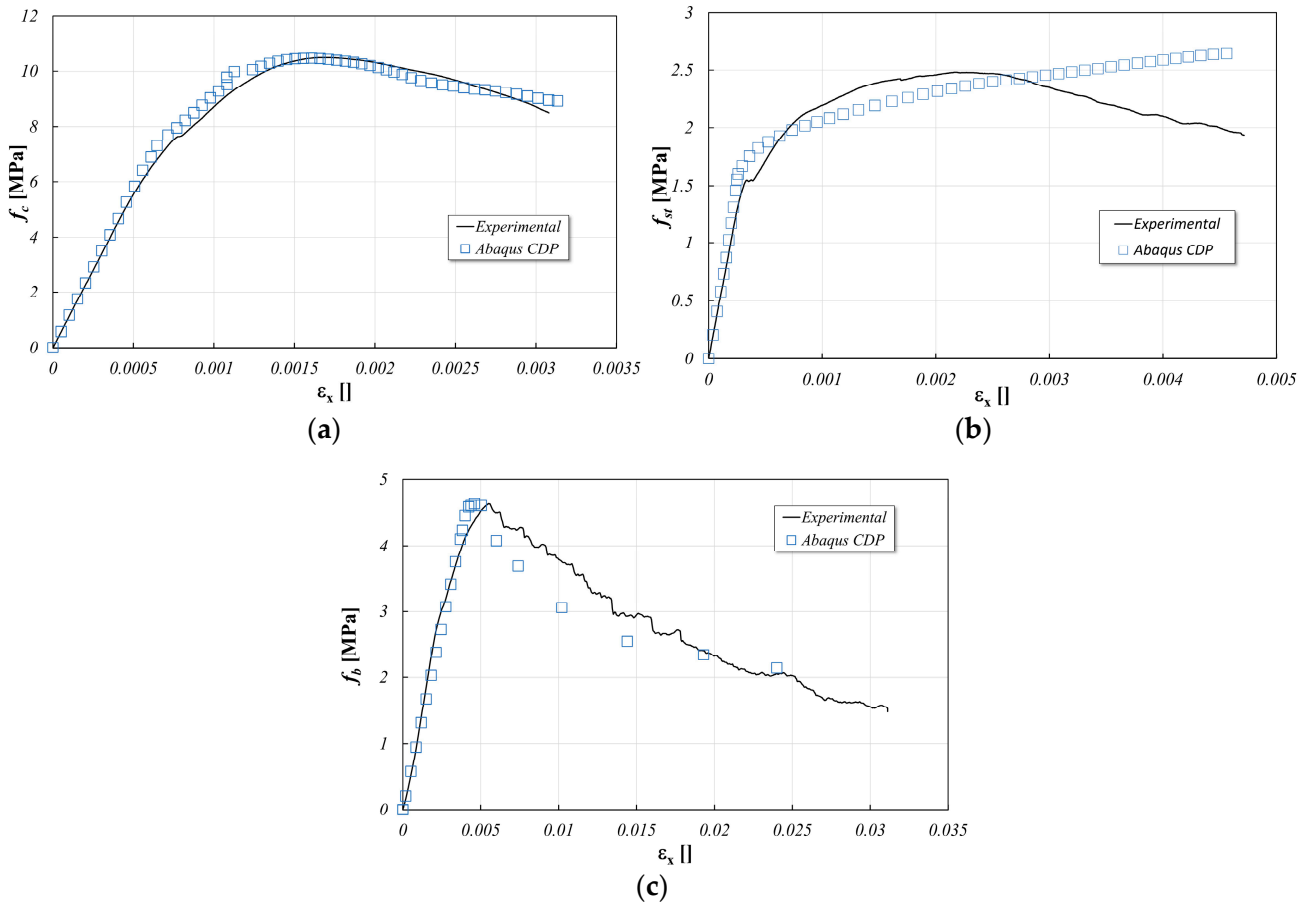

Figure 3. Comparison between experimental and numerical results: (**a**) compression test; (**b**) splitting test; (**c**) three-point bending test.

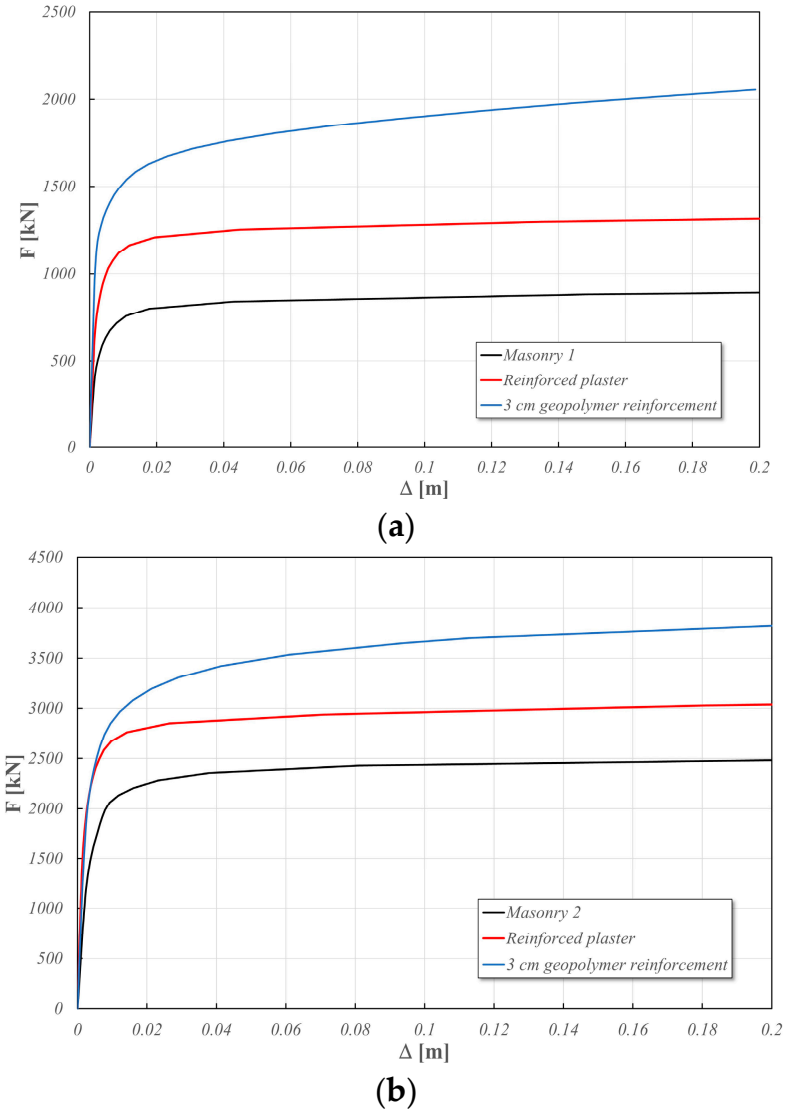

Figure 4. $F-\Delta$ curves: (**a**) Masonry 1; (**b**) Masonry 2.

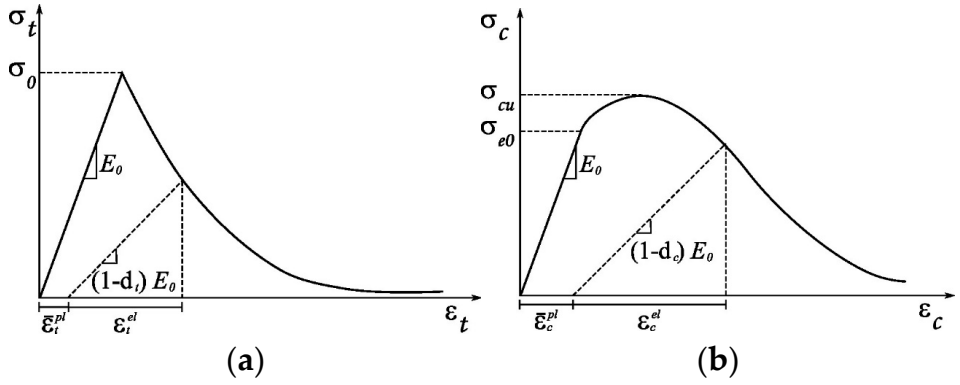

Figure 5. Definition of damage parameters: (**a**) d_t; (**b**) d_c.

In Figure 6, for Masonry 1, the d_c parameter at different load levels is reported; these figures are grouped by column: in the first column, the sketched maps are related to the original panel, those in the second column are related to the standard reinforced panel and those in the third column are related to the panel reinforced with the proposed plaster. In Figure 7, for Masonry 1, analogous maps are sketched for the d_t parameter.

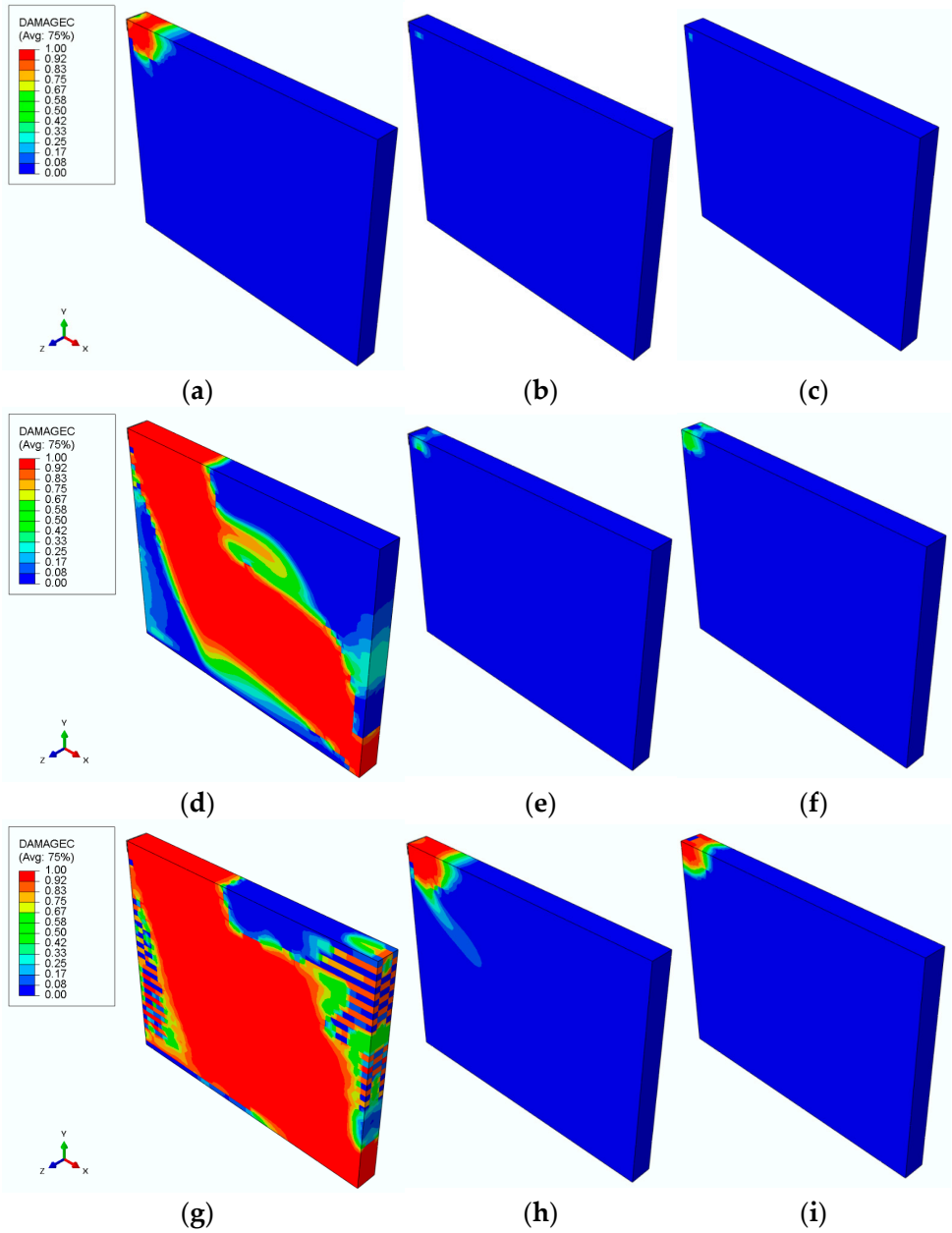

Figure 6. Maps of d_c parameter for Masonry 1. (**a–c**): $F = 680$ kN; (**d–f**): $F = 880$ kN; (**g–i**): $F = 1000$ kN.

The analysis of Figures 6 and 7 confirms that both the standard reinforced plaster and the plaster with the sisal fiber-reinforced geopolymer exert a positive effect on the masonry since the damage in the original masonry is greater for all force levels. Further, the proposed plaster shows damage less than that of the reinforced one, confirming its mechanical efficacy. It must be noted that in the last row of Figures 6 and 7, the sketched maps refer to a load level outside that reported in the pushover curves in Figure 5, which have been cropped only for clarity's sake.

To show the better structural effect of the proposed plaster with respect to the reinforced one, the maps of the d_c and d_t parameters at $F = 1400$ kN are reported in Figure 8 for both cases. An examination of these figures strongly confirms that in the case of the proposed plaster, the damage (both in terms of compression and tension) arising in the masonry is less than that suffered when the standard reinforced plaster is adopted.

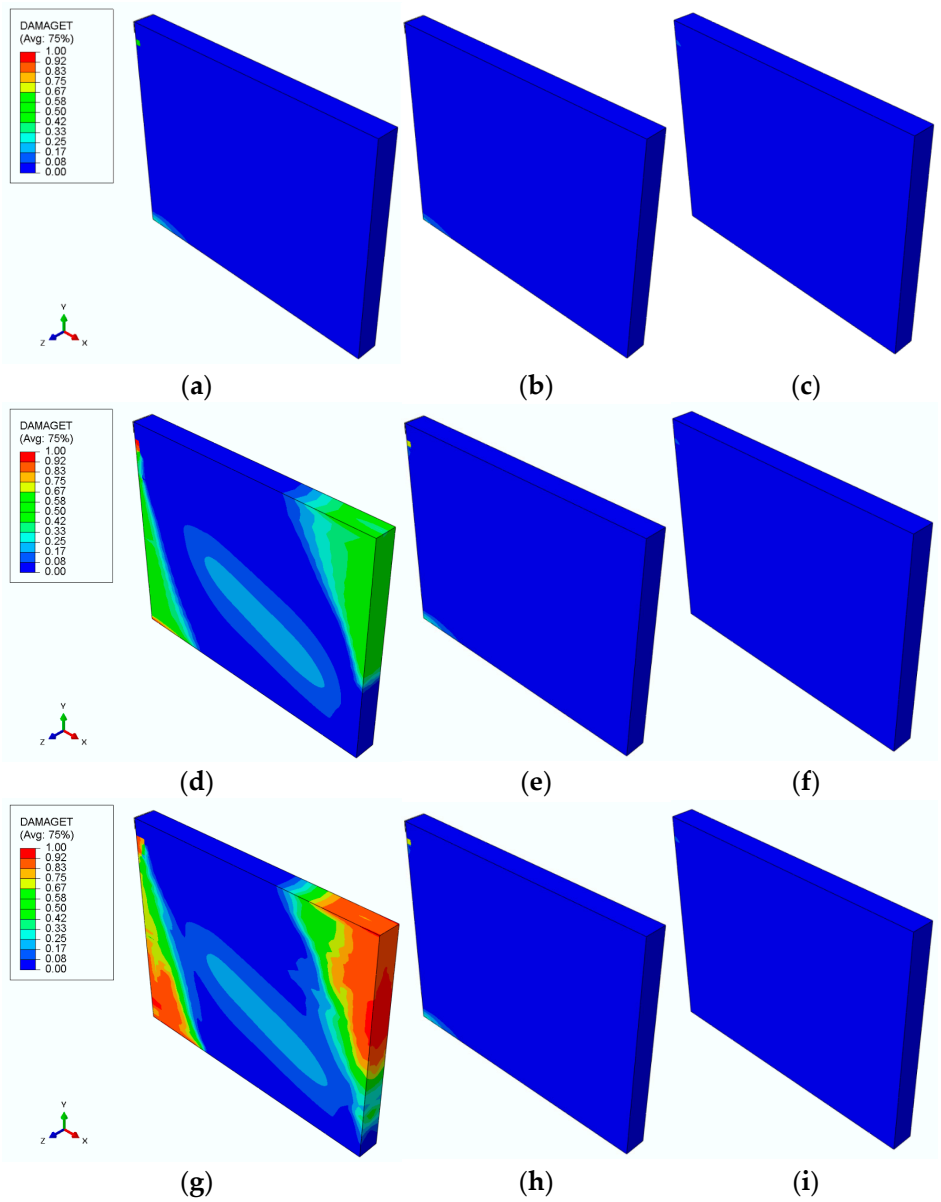

Figure 7. Maps of d_t parameter for Masonry 1. (**a–c**): $F = 680$ kN; (**d–f**): $F = 880$ kN; (**g–i**): $F = 1000$ kN.

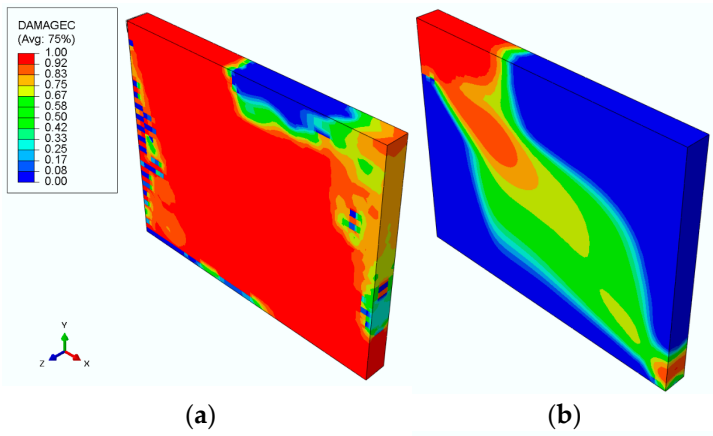

Figure 8. *Cont.*

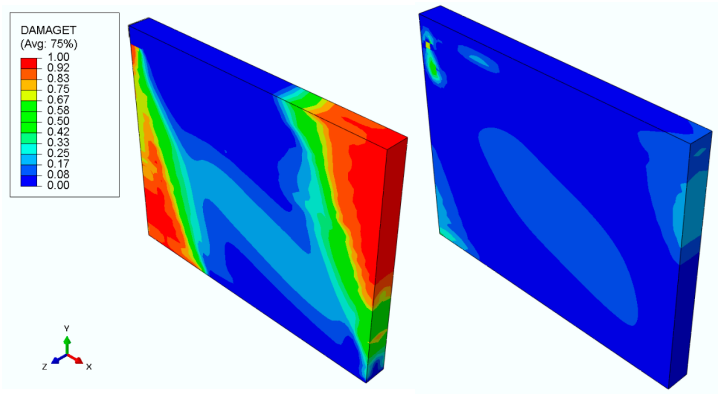

(**c**) (**d**)

Figure 8. Maps of damage parameters for Masonry 1 at $F = 1400$ kN: (**a**) d_c for reinforced plaster; (**b**) d_c for sisal fiber-reinforced plaster; (**c**) d_t for reinforced plaster; (**d**) d_t for sisal fiber-reinforced plaster.

Analogous results have been obtained for Masonry 2 and they are reported in Figures 9 and 10, while in Figure 11, the maps of the d_c and d_t parameters at $F = 3800$ kN are reported both for the standard reinforced plaster and for the proposed one.

The examination of these figures leads to the following remarks: (1) as in the case of Masonry 1, both interventions lead to an improvement in the mechanical behavior of the masonry panel, since at fixed load levels, the damage in the panel with interventions is reduced with respect to that in the original panel; (2) from a mechanical point of view, for a high-level load, the panel with the proposed plaster behaves better than that with the standard reinforced one since (see Figure 11) the damage levels suffered by the masonry are minor. The above remarks confirm the mechanical efficacy of the proposed plaster as an intervention for the strengthening of masonry structures.

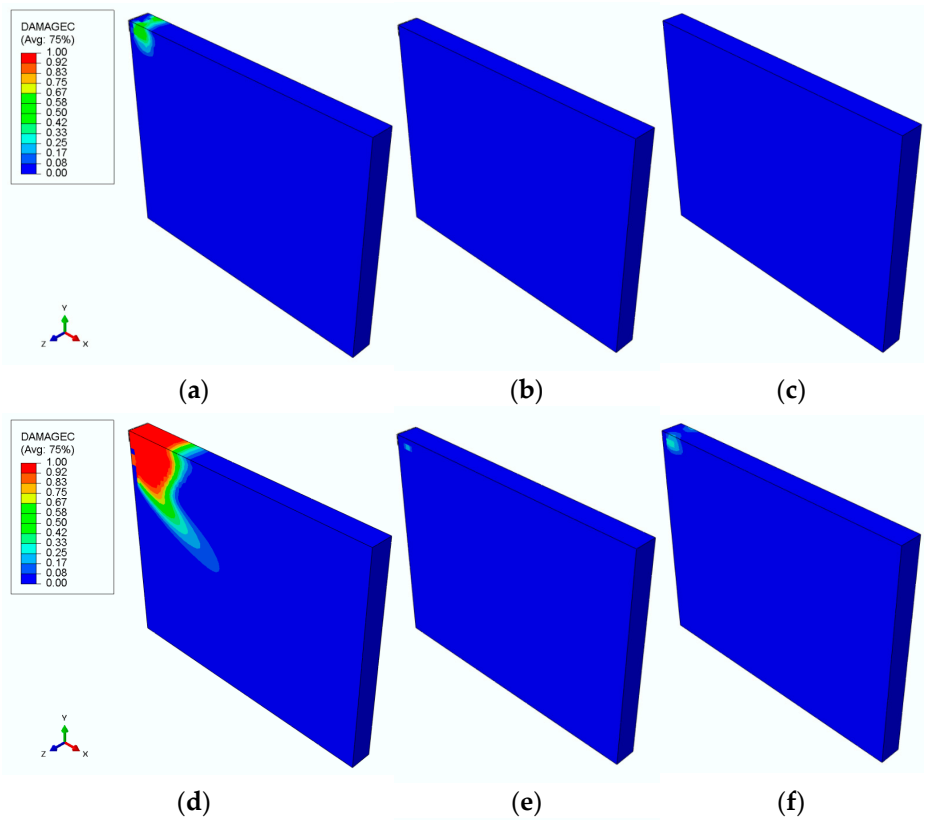

(**a**) (**b**) (**c**)

(**d**) (**e**) (**f**)

Figure 9. *Cont.*

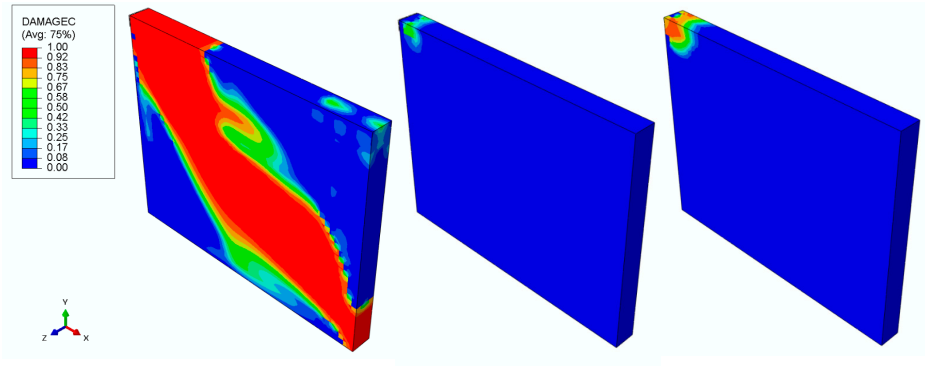

(**g**) (**h**) (**i**)

Figure 9. Maps of d_c parameter for Masonry 2. (**a–c**): $F = 2000$ kN; (**d–f**): $F = 2400$ kN; (**g–i**): $F = 2800$ kN.

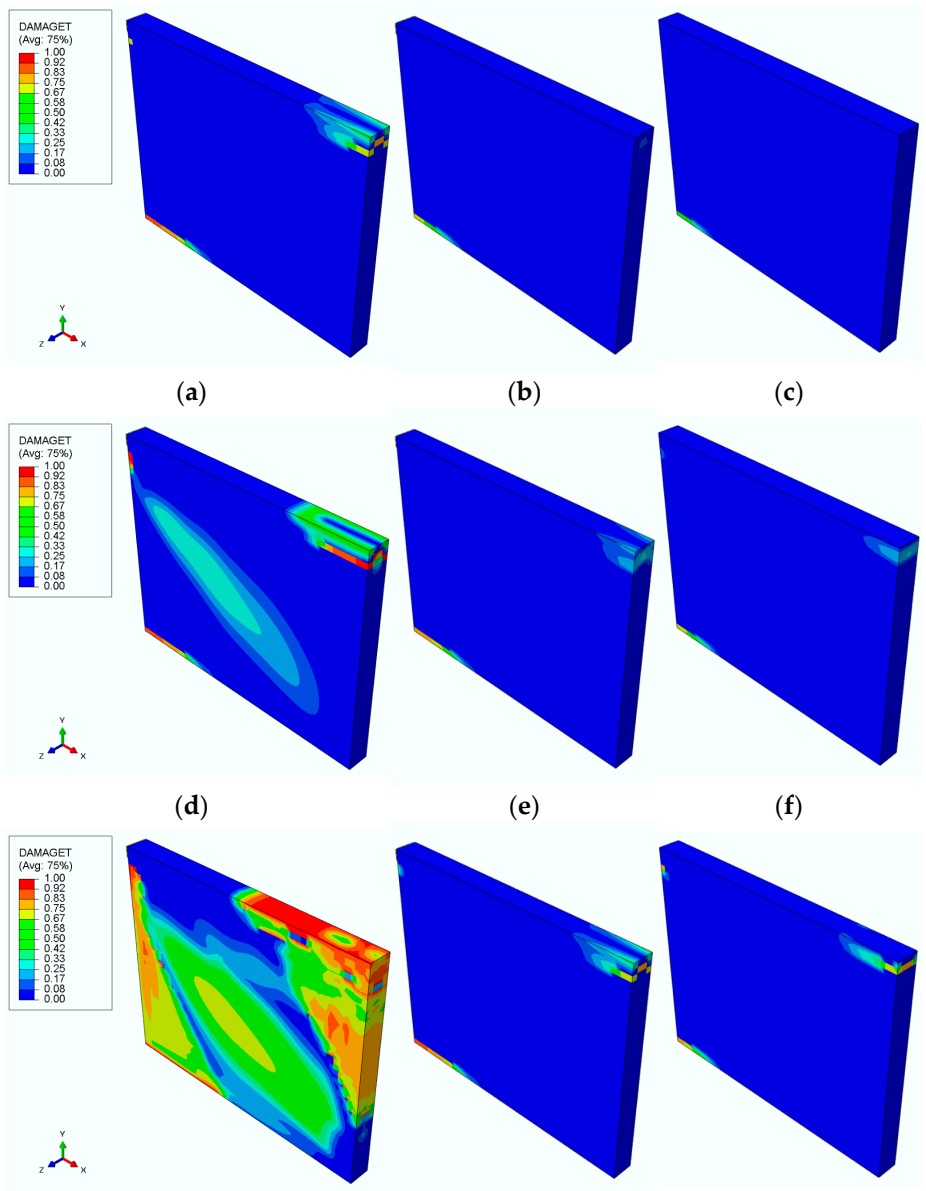

(**a**) (**b**) (**c**)

(**d**) (**e**) (**f**)

(**g**) (**h**) (**i**)

Figure 10. Maps of d_t parameter for Masonry 2. (**a–c**): $F = 2000$ kN; (**d–f**): $F = 2400$ kN; (**g–i**): $F = 2800$ kN.

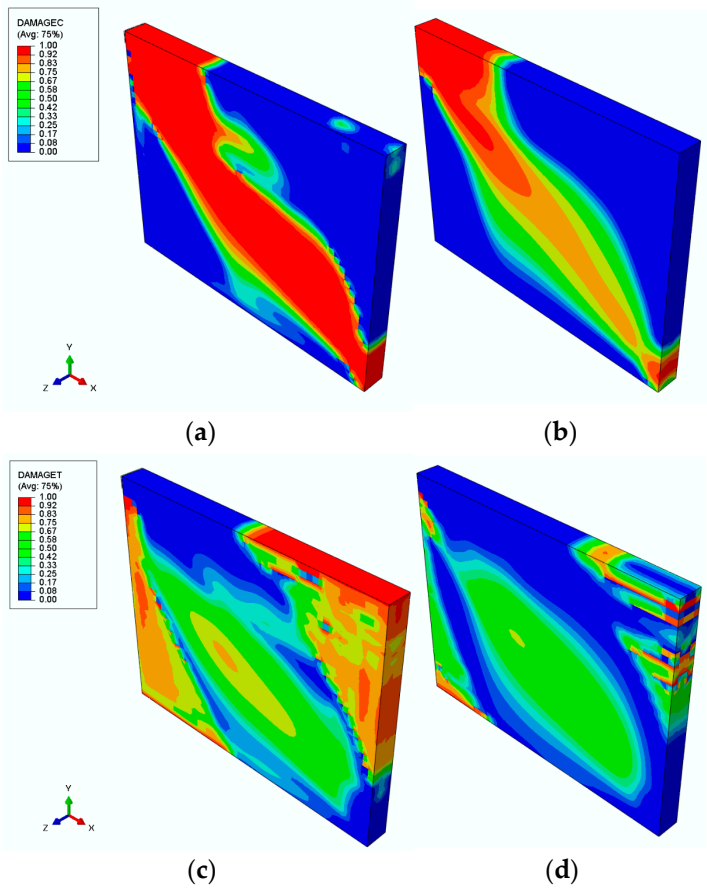

Figure 11. Maps of damage parameters for Masonry 2 at $F = 3000$ kN: (**a**) d_c for standard reinforced plaster; (**b**) d_c for sisal fiber-reinforced plaster; (**c**) d_t for standard reinforced plaster; (**d**) d_t for sisal fiber-reinforced plaster.

The analysis of the obtained results leads to the following remarks: (1) the original masonry panels (i.e., without strengthening) are very sensitive to lateral loads and the materials suffer high damage levels for relative low acting loads; (2) the strengthening layer (both the standard or proposed one) with suitable mechanical characteristics constitutes a layer able to absorb the main part of the stresses due to the acting loads greatly limiting the stresses acting on the original panel; (3) as a result, the presence of the strengthening layer leads to an increment in the ultimate load for the panel; (4) the mechanical characteristics of the material constituting the strengthening layer, especially the compressive and tensile strengths, are fundamental to obtain the expected result; (5) the stitching effect due to the fibers in the proposed reinforced plaster is the reason for the good mechanical behavior of the panel with such reinforcement.

4. Conclusions

In this paper, the possible use of sisal fiber-reinforced geopolymer plaster to improve the mechanical and structural behavior of masonry panels is presented. Initially, the experimental results of the mechanical tests performed on the samples of 2% w.t. sisal fiber-reinforced mortar were numerically modeled by assuming a concrete damage plasticity model, available in the ABAQUS library, to obtain the necessary information to be adopted in the subsequent analysis. Similarly, for masonry panels with and without reinforcement, the mechanical performance was determined by considering two different reinforcements and masonry typologies: sisal fiber-reinforced geopolymer plaster (0.03 m thickness with 2% w.t. sisal fibers) and the standard reinforced plaster referred to in structural regulations. The numerical results are expressed both in terms of pushover $F-\Delta$ curves and in terms of maps of the damage of the masonry. The latter are expressed by means of the output

parameters arising from the numerical material model adopted in the analyses. The obtained results show that the proposed plaster leads to an increment in the ultimate load bearable by the masonry and to lower material damage levels both in terms of compression and tension. Further benefits to be considered in the selection of the strengthening method are that the sisal fiber-reinforced geopolymer is very effective from a sustainability point of view. This aspect, together with a broader experimental campaign on real panels, and the related numerical analysis will be the topic of future works where the actual questions (the perfect adhesion between the mortar and masonry and the improvement in the numerical model of the reinforced plaster) will be explored more deeply.

Author Contributions: Conceptualization, S.B., L.P. and C.S.; numerical validation, S.B.; experimental investigation, S.B. and C.S.; writing—original draft preparation, S.B., C.S. and S.U.; writing—review and editing, S.B., L.P. and C.S.; supervision, L.P. All authors have read and agreed to the published version of the manuscript.

Funding: This research received no external funding.

Institutional Review Board Statement: Not applicable.

Informed Consent Statement: Not applicable.

Data Availability Statement: The original contributions presented in the study are included in the article, further inquiries can be directed to the corresponding author.

Conflicts of Interest: The authors declare no conflicts of interest.

References

1. Carbonara, G. *Atlante del Restauro*; UTET: Torino, Italy, 2004; t. I, sez. B e C; ISBN 9788802061207.
2. Cangi, G. *Manuale del Recupero Strutturale E Antisismico*; DEI: Milan, Italy, 2012; ISBN 9788849604399.
3. Cangi, G. *Manuale del Consolidamento E Restauro: Archi E Volte*; Tecniche costruttive, dissesti e interventi; DEI: Milan, Italy, 2023; ISBN 979-1255050032.
4. Varagnoli, C. *Muri Parlanti. Prospettive per L'analisi E la Conservazione Dell'edilizia Tradizionale*; Alinea: Milano, Italy, 2010; ISBN 8860554802.
5. D'Ayala, D.F.; Paganoni, S. Assessment and analysis of damage in L'Aquila historic city centre after 6th April 2009. *Bull. Earth. Eng.* **2011**, *9*, 81–104. [CrossRef]
6. Giuriani, E.; Marini, A.; Porteri, C.; Preti, M. Seismic vulnerability for churches in association with transverse arch rocking. *Int. J. Arch. Herit.* **2009**, *3*, 212–234. [CrossRef]
7. Gokhfeld, D.A.; Cherniavsky, D.F. *Limit Analysis of Structures at Thermal Cycling*; Springer: Dordrecht, The Netherlands, 1980; ISBN 978-90-286-0455-1.
8. Benfratello, S.; Palizzolo, L.; Tabbuso, P. Probabilistic Evaluation of the Adaptation Time for Structures under Seismic Loads. *Proc. Eng.* **2016**, *161*, 434–438. [CrossRef]
9. Benfratello, S.; Di Paola, M.; Palizzolo, L.; Tabbuso, P. Evaluation of the shakedown limit load multiplier for stochastic seismic actions. *Meccanica* **2017**, *52*, 2735–2750. [CrossRef]
10. Chen, W.; Duan, L. *Plasticity, Limit Analysis, Stability and Structural Design: An Academic Life Journey from Theory to Practice*; World Scientific: Singapore, 2021; ISBN 978-981122974-9/978-981122973-2.
11. Banichuk, N.V. *Introduction to Optimization of Structures*; Springer: New York, NY, USA, 1990; ISBN 978-1-4612-7988-4. [CrossRef]
12. Benfratello, S.; Giambanco, F.; Palizzolo, L.; Tabbuso, P. Structural design of frames able to prevent element buckling. In Proceedings of the 11th International Conference on Computational Structures Technology, CST 2012, Civil-Comp Proceedings, Dubrovnik, Croatia, 4–7 September 2012; Code 102644. Volume 99, ISBN 978-190508854-6.
13. Benfratello, S.; Palizzolo, L.; Tabbuso, P. Optimization of structures with unrestricted dynamic shakedown constraints. *Struct. Mult. Opt.* **2015**, *52*, 431–445. [CrossRef]
14. Zhang, R.; Hu, S. Optimal design of self-centering braced frames with limited self-centering braces. *J. Build. Eng.* **2024**, *88*, 109201. [CrossRef]
15. Faella, C.; Martinelli, E.; Nigro, E.; Paciello, S. Shear capacity of masonry walls externally strengthened by a cement-based composite material: An experimental campaign. *Constr. Build. Mater.* **2010**, *24*, 84–93. [CrossRef]
16. Gams, M.; Boem, I.; Gattesco, N.; Rizzi, E.; Dudine, A. Experimental study on the seismic enhancement of brick masonry spandrels using a single-sided composite reinforced mortar coating. *Bull. Earth. Eng.* **2024**, *22*, 2531–2552. [CrossRef]
17. Capozucca, R.; Magagnini, E. Historical masonry wallets with plaster slabs strengthened by CrFRM and GFRP. *Int. J. Mas. Res. Innov.* **2023**, *8*, 373–396. [CrossRef]

18. Benfratello, S.; Cucchiara, C.; Palizzolo, L.; Tabbuso, P. Fixed strength and stiffness hinges for steel frames. In Proceedings of the AIMETA 2017—Proceedings of the 23rd Conference of the Italian Association of Theoretical and Applied Mechanics, AIMETA 2017, Salerno, Italy, 4–7 September 2017; Volume 1, pp. 1287–1296, Code 133541, ISBN 978-889424847-0.
19. Benfratello, S.; Palizzolo, L. Limited resistance rigid perfectly plastic hinges for steel frames. *Int. Rev. Civ. Eng.* **2017**, *8*, 286–298. [CrossRef]
20. Billi, L.; Laudicina, F.; Salvatori, L.; Orlando, M.; Spinelli, P. Forming new steel-framed openings in load-bearing masonry walls: Design methods and nonlinear finite element simulations. *Bull. Earth. Eng.* **2019**, *5*, 2647–2670. [CrossRef]
21. Benfratello, S.; Palizzolo, L.; Tabbuso, P.; Vazzano, S. On the post elastic behavior of LRPH connections. *Int. Rev. Model. Simul.* **2019**, *12*, 341–353. [CrossRef]
22. Oña Vera, M.Y.; Metelli, G.; Barros, J.A.O.; Plizzari, G.A. Behaviour of steel frames infilled with environmentally and structurally favourable masonry units. *Eng. Struct.* **2020**, *204*, 109909. [CrossRef]
23. Benfratello, S.; Palizzolo, L.; Tabbuso, P.; Vazzano, S. LRPH device optimization for axial and shear stresses. *Int. Rev. Civ. Eng.* **2020**, *11*, 152–163. [CrossRef]
24. Benfratello, S.; Caddemi, S.; Palizzolo, L.; Pantò, B.; Rapicavoli, D.; Vazzano, S. Targeted steel frames by means of innovative moment resisting connections. *J. Constr. Steel Res.* **2021**, *183*, 106695. [CrossRef]
25. Sbrogiò, L.; Saretta, Y.; Valluzzi, M.R. Modelling of in-plane strengthening of unreinforced masonry buildings: A numerical comparison between traditional and FRCM jacketing. *Int. J. Mas. Res. Innov.* **2023**, *9*, 96–125. [CrossRef]
26. Roca, P. The Iscarsah Guidelines on the Analysis, Conservation and Structural Restoration of Architectural Heritage. Available online: https://www.scipedia.com/public/Roca_2021a (accessed on 30 November 2021).
27. Gattesco, N.; Boem, I. Experimental and analytical study to evaluate the effectiveness of an in-plane reinforcement for masonry walls using GFRP meshes. *Constr. Build. Mater.* **2015**, *88*, 94–104. [CrossRef]
28. Kalali, A.; Kabir, M.Z. Experimental response of double-wythe masonry panels strengthened with glass fiber reinforced polymers subjected to diagonal compression tests. *Eng. Struct.* **2012**, *39*, 24–37. [CrossRef]
29. Thomoglou, A.K.; Jagadesh, P.; Voutetaki, M.E. Review of Out-of-Plane Strengthening Techniques of Unreinforced Masonry Walls. *Fibers* **2023**, *11*, 78. [CrossRef]
30. Giaretton, M.; Dizhur, D.; da Porto, F.; Ingham, J.M. Seismic assessment and improvement of unreinforced stone masonry buildings: Literature review and application to New Zealand. *Bull. N. Z. Soc. Earth. Eng.* **2016**, *49*, 148–174. [CrossRef]
31. Corradi, M.; Borri, A.; Castori, G.; Sisti, R. The Reticulatus method for shear strengthening of fair-faced masonry. *Bull. Earth. Eng.* **2016**, *14*, 3547–3571. [CrossRef]
32. Borri, A.; Corradi, M.; Sisti, R.; Buratti, C.; Belloni, E.; Moretti, E. Masonry wall panels retrofitted with thermal-insulating GFRP-reinforced jacketing. *Mat. Struct.* **2016**, *49*, 3957–3968. [CrossRef]
33. Valluzzi, M.R.; Binda, L.; Modena, C. Mechanical behaviour of historic masonry structures strengthened by bed joints structural repointing. *Constr. Build. Mater.* **2005**, *19*, 63–73. [CrossRef]
34. Oliveira, D.V.; Silva, R.A.; Garbin, E.; Lourenço, P.B. Strengthening of three-leaf stone masonry walls: An experimental research. *Mat. Struct.* **2012**, *45*, 1259–1276. [CrossRef]
35. Morgan, D.R.; Jolin, M. *Shotcrete: Materials, Performance and Use*; CRC Press: Boca Raton, FL, USA, 2022.
36. Xuan-Bach, L.; Sang Mook, H. Experimental and analytical investigation of RC beams strengthened by ultra-high performance shotcrete. *Eng. Struct.* **2024**, *317*, 118642. [CrossRef]
37. Tarhan, I.H.; Uysal, H. Topology Optimization of the FRP for strengthening of masonry barrel vaults. *Eng. Fail. Anal.* **2023**, *151*, 107390. [CrossRef]
38. Kocaman, I.; Gürbüz, M. Enhancing seismic performance of historic mosques through retrofitting measures. *Eng. Struct.* **2024**, *301*, 117245. [CrossRef]
39. Bhattacharya, S.; Nayak, S.; Dutta, S.C. A critical review of retrofitting methods for unreinforced masonry structures. *Int. J. Dis. Risk Red.* **2014**, *7*, 51–67. [CrossRef]
40. Cominelli, S.; Giuriani, E.; Marini, A. Mechanisms governing the compressive strength of unconfined and confined rubble stone masonry. *Mat. Struct.* **2017**, *50*, 10. [CrossRef]
41. Corradi, M.; Borri, A.; Castori, G.; Sisti, R. Shear strengthening of wall panels through jacketing with cement mortar reinforced by GFRP grids. *Compos. B Eng.* **2014**, *64*, 33–42. [CrossRef]
42. Gioffrè, M.; Pepi, C. Environmental aging effects on mechanical behavior of an hemp based biocomposite material for structural strengthening. *J. Build. Eng.* **2024**, *91*, 109571. [CrossRef]
43. Coppola, L.; Coffetti, D.; Crotti, E. Pre-packed alkali activated cement-free mortars for repair of existing masonry buildings and concrete structures. *Constr. Build. Mater.* **2018**, *173*, 111–117. [CrossRef]
44. Jang, J.G.; Lee, N.K.; Lee, H.K. Fresh and hardened properties of alkali-activated fly ash/slag pastes with superplasticizers. *Constr. Build. Mater.* **2014**, *50*, 169–176. [CrossRef]
45. Shahrajabian, F.; Behfarnia, K. The effects of nano particles on freeze and thaw resistance of alkali-activated slag concrete. *Constr. Build. Mater.* **2018**, *176*, 172–178. [CrossRef]
46. Coppola, L.; Coffetti, D.; Crotti, E.; Gazzaniga, G.; Pastore, T. An Empathetic Added Sustainability Index (EASI) for cementitious based construction materials. *J. Clean. Prod.* **2019**, *220*, 475–482. [CrossRef]

47. Amran, Y.H.M.; Alyousef, R.; Alabduljabbar, H.; El-Zeadani, M. Clean production and properties of geopolymer concrete; A review. *J. Clean. Prod.* **2020**, *251*, 119679. [CrossRef]
48. Rajamane, N.P.; Nataraja, M.C.; Lakshmanan, N. An introduction to geopolymer concrete. *Ind. Concr. J.* **2011**, *85*, 25–28.
49. Mahmood, A.; Noman, M.T.; Pechočiaková, M.; Amor, N.; Petrů, M.; Abdelkader, M.; Militký, J.; Sozcu, S.; Hassan, S.Z.U. Geopolymers and Fiber-Reinforced Concrete Composites in Civil Engineering. *Polymers* **2021**, *13*, 2099. [CrossRef]
50. Ma, C.K.; Awang, A.Z.; Omar, W. Structural and material performance of geopolymer concrete: A review. *Constr. Build. Mater.* **2018**, *186*, 90–102. [CrossRef]
51. Guo, X.; Pan, X. Mechanical properties and mechanisms of fiber reinforced fly ash–steel slag based geopolymer mortar. *Constr. Build. Mater.* **2018**, *179*, 633–641. [CrossRef]
52. Longo, F.; Lassandro, P.; Moshiri, A.; Phatak, T.; Aiello, M.A.; Krakowiak, K.J. Lightweight geopolymer-based mortars for the structural and energy retrofit of buildings. *Energy Build.* **2020**, *225*, 110352. [CrossRef]
53. Abulencia, A.B.; Villoria, M.B.D.; Libre, R.G.D., Jr.; Quiatchon, P.R.J.; Dollente, I.J.R.; Guades, E.J.; Promentilla, M.A.B.; Garciano, L.E.O.; Ongpeng, J.M.C. Geopolymers as Sustainable Material for Strengthening and Restoring Unreinforced Masonry Structures: A Review. *Buildings* **2021**, *11*, 532. [CrossRef]
54. Corradi, M.; Mustafaraj, E.; Speranzini, E. Sustainability considerations in remediation, retrofit, and seismic upgrading of historic masonry structures. *Environ. Sci. Pollut. Res.* **2023**, *30*, 25274–25286. [CrossRef] [PubMed]
55. Huang, Y.; Tan, J.; Xuan, X.; Liu, L.; Xie, M.; Liu, H.; Yu, S.; Zheng, G. Study on untreated and alkali treated rice straw reinforced geopolymer composites. *Mater. Chem. Phys.* **2021**, *262*, 124304. [CrossRef]
56. Malenab, R.A.J.; Ngo, J.P.S.; Promentilla, M.A.B. Chemical treatment of waste abaca for natural fiber-Reinforced geopolymer composite. *Materials* **2017**, *10*, 579. [CrossRef]
57. Jabbar, A.; Militký, J.; Wiener, J.; Javaid, M.U.; Rwawiire, S. Tensile, surface and thermal characterization of jute fibres after novel treatments. *Indian J. Fibre Text. Res.* **2016**, *41*, 249–254.
58. Majumder, A.; Stochino, F.; Frattolillo, A.; Valdes, M.; Gatto, G.; Martinelli, E. Sustainable Retrofitting Solutions: Evaluating the Performance of Jute Fiber Nets and Composite Mortar in Natural Fiber Textile Reinforced Mortars. *Sustainability* **2024**, *16*, 1175. [CrossRef]
59. Fiore, V.; Calabrese, L. Effect of stacking sequence and sodium bicarbonate treatment on quasi-static and dynamic mechanical properties of flax/jute epoxy-based composites. *Materials* **2019**, *12*, 1363. [CrossRef]
60. Sukontasukkul, P.; Pongsopha, P.; Chindaprasirt, P.; Songpiriyakij, S. Flexural performance and toughness of hybrid steel and polypropylene fibre reinforced geopolymer. *Constr. Build. Mater.* **2018**, *161*, 37–44. [CrossRef]
61. Farooq, M.; Bhutta, A.; Banthia, N. Tensile performance of eco-friendly ductile geopolymer composites (EDGC) incorporating different micro-fibers. *Cem. Concr. Compos.* **2019**, *103*, 183–192. [CrossRef]
62. Ranjbar, N.; Talebian, S.; Mehrali, M.; Kuenzel, C.; Metselaar, H.S.C.; Zamin Jumaat, M. Mechanisms of interfacial bond in steel and polypropylene fiber reinforced geopolymer composites. *Compos. Sci. Technol.* **2016**, *122*, 73–81. [CrossRef]
63. Martinie, L.; Rossi, P.; Roussel, N. Rheology of fiber reinforced cementitious materials: Classification and prediction. *Cem. Concr. Res.* **2010**, *40*, 226–234. [CrossRef]
64. Mo, K.H.; Alengaram, U.J.; Jumaat, M.Z. Structural performance of reinforced geopolymer concrete members: A review. *Constr. Build. Mater.* **2016**, *120*, 251–264. [CrossRef]
65. Ranjbar, N.; Mehrali, M.; Mehrali, M.; Alengaram, U.J.; Jumaat, M.Z. High tensile strength fly ash based geopolymer composite using copper coated micro steel fiber. *Constr. Build. Mater.* **2016**, *112*, 629–638. [CrossRef]
66. Ranjbar, N.; Mehrali, M.; Behnia, A.; Javadi Pordsari, A.; Mehrali, M.; Alengaram, U.J.; Jumaat, M.Z. A Comprehensive Study of the Polypropylene Fiber Reinforced Fly Ash Based Geopolymer. *PLoS ONE* **2016**, *11*, e0147546. [CrossRef]
67. Asil, M.B.; Ranjbar, M.M. Hybrid effect of carbon nanotubes and basalt fibers on mechanical, durability, and microstructure properties of lightweight geopolymer concretes. *Constr. Build. Mater.* **2022**, *357*, 129352. [CrossRef]
68. Payakaniti, P.; Pinitsoontorn, S.; Thongbai, P.; Amornkitbamrung, V.; Chindaprasirt, P. Electrical conductivity and compressive strength of carbon fiber reinforced fly ash geopolymeric composites. *Constr. Build. Mater.* **2017**, *135*, 164–176. [CrossRef]
69. Rovnaník, P.; Šimonová, H.; Topolář, L.; Bayer, P.; Schmid, P.; Keršner, Z. Carbon nanotube reinforced alkali-activated slag mortars. *Constr. Build. Mater.* **2016**, *119*, 223–229. [CrossRef]
70. da Silva, A.C.R.; Mendes Almeida, B.; Moraes Lucas, M.; Scarpini Cândido, V.; Pinheiro da Cruz, K.S.; Souza Oliveira, M.; Rangel Garcez de Azevedo, A.; Neves Monteiro, S. Fatigue behavior of steel fiber reinforced geopolymer concrete. *Case Stud. Constr. Mat.* **2022**, *16*, e00829. [CrossRef]
71. Ardanuy, M.; Claramunt, J.; Dias Toledo Filho, R. Cellulosic fiber reinforced cement-based composites: A review of recent research. *Constr. Build. Mater.* **2015**, *79*, 115–128. [CrossRef]
72. Camargo, M.M.; Adefrs Taye, E.; Roether, J.A.; Tilahun Redda, D.; Boccaccini, A.R. A Review on Natural Fiber-Reinforced Geopolymer and Cement-Based Composites. *Materials* **2020**, *13*, 4603. [CrossRef] [PubMed]
73. Moujoud, Z.; Sair, S.; Ait Ousaleh, H.; Ayouch, I.; El Bouari, A.; Tanane, O. Geopolymer composites reinforced with natural Fibers: A review of recent advances in processing and properties. *Constr. Build. Mater.* **2023**, *388*, 131666. [CrossRef]
74. Greco, P.F.; Pepi, C.; Gioffré, M. A novel biocomposite material for sustainable constructions: Metakaolin lime mortar and Spanish broom fibers. *J. Build. Eng.* **2024**, *83*, 108425. [CrossRef]

75. Korniejenko, K.; Frączek, E.; Pytlak, E.; Adamski, M. Mechanical Properties of Geopolymer Composites Reinforced with Natural Fibers. *Proc. Eng.* **2016**, *151*, 388–393. [CrossRef]
76. Rajendran, M.; Bakthavatchalam, K.; Leela Bharathi, S.M. Review on the Hybridized Application of Natural Fiber in the Development of Geopolymer Concrete. *J. Nat. Fibers* **2023**, *20*, 2178578. [CrossRef]
77. Abdalla, J.A.; Hawileh, R.A.; Bahurudeen, A.; Jyothsna, G.; Sofi, A.; Shanmugam, V.; Thomas, B.S. A comprehensive review on the use of natural fibers in cement/geopolymer concrete: A step towards sustainability. *Case Stud. Constr. Mater.* **2023**, *19*, e02244. [CrossRef]
78. Benfratello, S.; Cirello, A.; Palizzolo, L.; Sanfilippo, C.; Valenza, A. Experimental Analysis and Numerical Modelling of the Mechanical Behavior of a Sisal-Fiber-Reinforced Geopolymer. *Appl. Sci.* **2024**, *14*, 5216. [CrossRef]
79. Ranjbar, N.; Zhang, M. Fiber-reinforced geopolymer composites: A review. *Cem. Concr. Compos.* **2020**, *107*, 103498. [CrossRef]
80. *EN 1015-11:2019*; Methods of Test for Mortar for Masonry—Part 11: Determination of Flexural and Compressive Strength of Hardened Mortar. European Committee for Standardization: Brussels, Belgium, 2019.
81. *ASTM D3967-16*; Standard Test Method for Splitting Tensile Strength of Intact Rock Core Specimens. ASTM International: West Conshohocken, PA, USA, 2023.
82. Elkady, A. *ABAQUS CDP Generator: A Tool for Generating Concrete Damage Parameters for ABAQUS*; v. 23.04; Zenodo: Geneva, Switzerland, 2023. [CrossRef]
83. *SIMULIA (2017) Abaqus Documentations*; Dassault Systems: Vélizy-Villacoublay, France, 2017.
84. *DM 17/01/2018*; Italian Ministry of Infrastructure and Transport, National Standard. NTC: Manila, Philippines, 2018.